

Impact of eddies on dissolved inorganic carbon components in the Bay of Bengal

V.V.S.S. Sarma, G. Sampath Kumar, K. Yadav, H.B. Dalabehera, D.N. Rao, S. Behera, J. Loganathan

CSIR-National Institute of Oceanography, Regional Centre,
176 Lawsons Bay Colony, Visakhapatnam – 530 017, India

*Corresponding author (sarmav@nio.org)

Abstract

To examine the influence of anticyclonic (ACE) and cyclonic (CE) eddies on variations in hydrographic properties and total inorganic carbon system (C_T), a study was conducted in the western Bay of Bengal (BoB). The depth of seasonal thermocline, defined as depth of 20°C isotherm (D20), shoaled (~80 m) in the CE but deepened to ~180 m in the ACE relative to non-eddy (NE) conditions (~110 m) due to convergence and divergence associated with ACE and CE, respectively. Both surface and depth integrated (0-100 m) chlorophyll-a concentrations were higher in CE than in ACE and NE regions suggesting higher primary production in the CE region. Upward displacement of 2100 μM of C_T and 800 μatm of $p\text{CO}_2$ isosurfaces from a depth of 175 to 50 m was observed in the CE region resulting in an increase in mixed layer C_T and $p\text{CO}_2$ compared to that in NE region. Low C_T (~1850 μM) and high pH (~8.15) isolines deepened to 150-175 m in ACE region. Strong positive relations were observed for C_T and $p\text{CO}_2$ with salinity whereas weak inverse correlations were found for chlorophyll-a and dissolved oxygen saturation with salinity normalized C_T . This suggests that both biological and physical processes control C_T in the BoB. Both biological and mixing effects contributed significantly to $p\text{CO}_2$ variability in the CE region whereas mixing and thermal effects contributed in the ACE region. The sea-to-air fluxes of CO_2 varied between -0.21 and 0.31 $\text{molC m}^{-2} \text{month}^{-1}$. The CE and south ACE (ACE_s) regions were found to act as sink for the atmospheric CO_2 whereas northern ACE (ACE_n) and NE regions were source. The mean CO_2 flux suggests that the study region was a moderate source ($0.05 \pm 0.01 \text{ molC m}^{-2} \text{month}^{-1}$) to the atmosphere. The mean sinking flux of C_T to the deeper layer in ACE_n and ACE_s was $\sim 0.07 \pm 0.02 \text{ molC m}^{-2} \text{month}^{-1}$ whereas it was $\sim 0.02 \pm 0.006 \text{ C m}^{-2} \text{month}^{-1}$ in CE and NE regions. Assuming that the estimated flux at the eddies sampled here is applicable to all eddies in the Bay, the vertical DIC flux to the deep BoB by all eddies amounted to $3.29 \pm 0.9 \text{ TgC y}^{-1}$ (1 $\text{TgC} = 10^{12} \text{ gC}$). Nevertheless this study suggests that ACEs transports C_T to deeper waters, besides being source to the atmospheric CO_2 .

Introduction

The coastal ocean is considered to be a major sink of the atmospheric carbon dioxide (CO₂) (IGBP, 1993). The magnitude of atmospheric CO₂ absorption is being altered due to anthropogenic interference (Bauer et al., 2013; Regnier et al., 2013). It has been estimated that ~1 PgC y⁻¹ (1 Pg=10¹⁵gC) of atmospheric CO₂ is absorbed by the global coastal ocean (Tsunogai et al. (1999). The revised estimations suggest that the CO₂ absorption by coastal ocean decreased to ~0.2 PgC y⁻¹ (Chen et al., 2013; Laruelle et al., 2014). These estimates suffer from significant uncertainties due to lack of data from the coastal regions, especially from the southeast and south Asian region (Borges, 2005).

The Bay of Bengal (BoB), the northeastern part of the Indian Ocean, is unique by geographical settings (closed on three sides and open to the Indian Ocean in the south), huge freshwater discharge (Sarma et al., 2012) from Himalayan and peninsular rivers (such as the Ganges, Brahmaputra, Irrawady, Godavari, Krishna, Mahanadi; UNESCO, 1979), seasonally reversing coastal currents (Murty et al., 1993; Shetye et al., 1996) and occurrence of seasonal coastal upwelling (Gopalakrishna and Sastry, 1985). The coastal circulation in the western BoB is dominated by the seasonally reversing currents and multiple meso-scale cyclonic (CE) and anticyclonic eddies (ACE). The seasonal currents constitute a poleward flowing East India Coastal Current (EICC) – also known as the Western Boundary Current (WBC; Shetye et al., 1993; Sanilkumar et al., 1997; Babu et al., 2003; Gangopadhyay et al., 2015). The WBC forms in January and well develops during March-April, and decays by June (Shetye et al., 1993). Kumar et al. (1996) measured for the first time total inorganic carbon (C_T) components in the BoB and found that BoB is a strong sink for the atmospheric CO₂ during pre-southwest (April-May) and winter (January-February) monsoon. Sarma et al. (2012) suggested that whether BoB acting as a sink or source during southwest monsoon (June to September) depends on the source of freshwater wherein the northern BoB acts as a significant sink but southern BoB is a source. Recently Sarma et al. (2015) noticed rapid acidification of the BoB during winter and spring due to deposition of atmospheric pollutants and found that the BoB acted as a source for the atmospheric CO₂ during 2014, while it was a sink during 1994. Occurrence of coastal upwelling, close to the coast, resulting in enhanced CO₂ fluxes to the atmosphere was reported (Sarma et al., 2015) and it has been further noticed that coastal upwelling intensified during the period of positive Indian Ocean Dipole.

Seasonal variations in C_T and pCO₂ in the northwestern Pacific Ocean are attributed to occurrence of eddies (Kimura, 1970; Rogachev et al., 1996; Kusakabe et al., 2002). Increase in C_T and pCO₂ levels associated with upward pumping in the CE was reported in several regions (Kusakabe et al., 2002;

Perez et al., 2001; Gonzalez-Davila et al., 2003; 2006). Enhanced anthropogenic carbon uptake associated with mesoscale eddies is reported for the global ocean (Gnanadesikan et al., 2015). Occurrence of strong mesoscale eddy activity is reported in the western BoB (Durand et al., 2009) due to both barotropic and baroclinic instability of the mean current (Cheng et al. 2013). Babu et al. (2003) identified the WBC as a meandering northward flowing current in April 1987 and the occurrence of two CEs to the inshore of WBC. Gangopadhyay et al. (2015), using satellite altimetry based absolute dynamic height maps during 2000-2010 and model simulations and Ertel's potential vorticity considerations, presented evidence that the WBC is a continuous northward-flowing current from about 12°N to 17°N that moves away from the coast at 18°N during spring. These authors also noticed inter-annual variability in the flow pattern of the meandering WBC from 8°N to 18°N in April from 2000 to 2010, with the dominance of ACE in some years and their absence in the other. Sarma et al. (2015) showed that the EICC, south of 17°N, is dominantly equatorward during November-December 2013, which is a poleward coastal current associated with an ACE north of 17°N. Chen et al. (2012) reported that as many as ~10 eddies form in the northern BoB per 1° grid and that their frequency decreased towards south (south of 5° N) due to weakening of Coriolis force that is required to maintain their dynamic balance. Dandapath and Chakraborty (2016) found that ACE are generally larger in size than CE and that the number of ACE is higher than that of CE in the BoB. Significant work was carried out on the role of CEs on primary production and nutrient inputs in the BoB (Prasanna Kumar et al., 2004; Narvekar and Prasanna Kumar, 2007) and increase in sinking carbon fluxes to the deep BoB (Vidya and Prasanna Kumar, 2013). However, the role of CE and ACE on variations in C_T components and fluxes of CO_2 in the BoB is unknown. The objective of this study is to examine the impact of eddies on C_T components and evaluate CO_2 fluxes in the western BoB.

2. Material and methods

2.1. Sampling

A cruise was undertaken in the BoB along the east coast of India, covering one CE, two ACEs and NE regions. Sampling was conducted at 22 stations from 23 March to 6 April 2018 (Fig. 1). Water column pressure, temperature and salinity (SBE 911 plus, USA), chlorophyll-a fluorescence (Wet Labs, USA) and dissolved oxygen (SBE 43, USA) were measured using sensors attached to Rosette (SBE 32, Sea-Bird, USA). The accuracies of these sensors are ± 1.0 db, $\pm 0.001^\circ C$, ± 0.002 , ± 0.01 mg m^{-3} and ± 2 μM respectively, based on measurements in the laboratory. The sampling was carried out in the upper 500 m of water column at standard depths using 10L Niskin bottles attached to the CTD rosette.

Bubble-free water samples were first collected for dissolved oxygen (DO), C_T , and pH. The DO was measured using Winkler titration method with endpoint detection (Carpenter, 1966) using a potentiometer (Titrande Metrohm, Zofingen, Switzerland). A 2-L water sample was filtered through a GF/F filter (0.7 μm pore size; Whatman) and chlorophyll a (Chl-*a*) retained on the filter was first extracted with N,N-dimethylformamide (DMF), kept at 4° C in the dark for 12 h and then spectrofluorometrically analyzed (Varian Eclipse fluorophotometer) following Suzuki and Ishimaru (1990). The analytical precision of Chl-*a* was $\pm 0.04 \text{ mg m}^{-3}$. The concentrations of nutrients were measured following standard spectrophotometric procedures using an autoanalyzer (Technicon; Taacs, Australia) (Grasshoff et al. 1983). The detection limits for nitrate, phosphate, and silicate were ± 0.05 , ± 0.02 , and $\pm 0.03 \text{ }\mu\text{M}$, respectively. The pH was measured using glass electrodes (Metrohm, Zofingen, Switzerland) following standard operating procedures suggested by the Department of Energy (DOE, 1998). C_T was measured using a coulometer (model CM 5014; UIC Inc., Joliet, IL, USA) attached to an automated sample-extraction system (Sarma, 1998; 2012; 2015). The precisions for pH, and C_T were ± 0.002 , and $\pm 1.8 \text{ }\mu\text{M}$, respectively. The accuracy of the pH and C_T was estimated using Certified Reference Material supply by Dr. A.G. Dickson of Scripps Institute of Oceanography, USA as 0.015 and 4 μM respectively. The pCO_2 was computed using the measured salinity, temperature, nutrients (phosphate and silicate), pH and C_T using the CO_2 SYS programme (Lewis and Wallace, 1998) and applying the CO_2 dissociation constants given by Millero et al. (2006) for the 0-40 salinity range. The uncertainty of the estimated pCO_2 is $\sim 7 \text{ }\mu\text{atm}$. The air-water flux of CO_2 was estimated using formulations given by Wanninkhof (2014) based on surface pCO_2 levels and daily mean wind speeds measured on board research vessel using an automated weather station at 10 m above sea level and atmospheric pCO_2 values obtained from CDIAC (http://cdiac.esd.ornl.gov/pns/current_ghg.html). The depth of mixed layer was estimated as the depth at which the density of water increased by 0.125 from at the surface.

2.2. Satellite Data

Surface features of the study region were mapped using the satellite information, including weekly mean (24 to 30th March 2018) sea surface temperature (SST; $0.04 \times 0.04^\circ$ degree; MODIS AQUA L3), sea surface salinity (SSS; $0.5 \times 0.5^\circ$ degree; AQUARIUS), sea surface height anomaly (SSHA; $0.25 \times 0.25^\circ$ degree), and geostrophic currents ($0.25 \times 0.25^\circ$ degree; Merged product) obtained from Copernicus Marine Environmental Monitoring Service (www.marine.copernicus.eu). Due to large data gaps, the monthly mean (1-31st March 2018) surface Chl-*a* data was presented from MODIS-Aqua ($0.04 \times 0.04^\circ$ degree; Figure 1). Monthly mean Advanced Scatterometer winds (ASCAT) data (las.incois.gov.in) were used to compute CO_2 fluxes.

3. Results

3.1. Surface remote sensing features

Figure 1 shows weakly mean of surface properties of sea surface height anomaly (SSHA), sea surface temperature (SST), sea surface salinity (SSS) and sea surface Chl-*a* during the study period. An eddy is identified based on the circulation of water and SSHA. The ACE is identified where anticyclonic circulation occurs associated with positive and higher than 0.2m of SSHA and vice versa for CE. The BoB is occupied by several ACEs of width ranging from 400 - 600 km and 50 - 150 km for CE during the study period (Fig. 1a). Satellite SST and SSS suggest occurrence of significantly low temperature and high salinity associated with CE (Fig. 1b,c). The surface salinity in the northern BoB (north of 15°N), was lower than that in the southern part of the bay (Fig. 1c). The low-salinity water in the north was colder compared to that in the south and east (Fig. 1b). Up to 30% of the BoB was occupied with variable sizes and intensities of ACEs. The strength of CEs was relatively weaker than ACEs, except in the northern BoB (Fig. 1a). Our cruise transect passed through two ACEs and one CE in the western BoB. The CE occurred near 200-550 km along the track distance, and ACEs at 600-1100 km and 1550- 2500 km and these, hereafter, are termed as northern (ACE_n) and southern ACE (ACE_s) respectively (Fig. 2). Higher SSHA by up to 0.3 m was observed within the core of the ACEs (Fig. 1a). The CE was also marked by a patch of elevated Chl-*a* at the surface (Fig. 1d). Relatively higher Chl-*a* was also observed in the non-eddy (NE) region between ACE_n and ACE_s (Fig. 1d)

3.2. Influence of eddies on hydrographic properties of water column

Water column between 40 and 100 m was warmer (by 2-8° C) and less salty (0.5-1.2) in the ACE_n and ACE_s than in CE and NE whereas low saline water was observed in the upper 40 m of water column in the CE and ACE_n regions (Fig 2a and b). The depth of seasonal thermocline, defined as depth of 20° C isotherm (D20), represents the mixing of upper water column, was located at ~80 m in the CE and the same was deepened to ~180 m in the ACE_n and ~150 m at ACE_s (~150 m) (Fig. 2a). Deepening of 34.5 isohaline was observed to 170 m in the ACE_n from that of 50 m in the NE region, but it was at ~125 m in the ACE_s (Fig. 2b). The depth of mixed layer varied between 6 and 34 m and it was shallow in the CE (10±2 m) and NE (14±1 m) than in ACE_n (23±2 m) and ACE_s (28±3) (Fig. 3).

Relatively higher Chl-*a* was observed in the upper 25 m of the water column in the CE region (0.12 mg m⁻³) than in ACE_n (0.05 mg m⁻³), ACE_s (0.04 mg m⁻³) and NE regions (0.08 mg m⁻³) (Fig. 2c). A prominent subsurface Chl-*a* maximum (SCM) was observed in the entire study region at shallower

depth in the CE (~44m) than in the ACE_n (64 m), ACE_s (82 m) and NE (58 m; Fig. 2c). Higher Chl-a in the SCM was observed in the CE than in ACEs and NE regions. The depth integrated (up to 100 m) Chl-a varied between 19.8 and 36.8 mg m⁻² and it was higher in the CE (32.6 mg m⁻²) compared to that in NE (27.5 mg m⁻²), ACE_n (23.6 mg m⁻²) and ACE_s (22.5 mg m⁻²) regions (Fig. 3). The mean vertical profiles of temperature, salinity, Chl-a, salinity normalized C_T, pH and pCO₂ in the CE, NE, ACE_n and ACE_s were presented in Figure 4 a-f. Figure 4 suggests that upper 300 m of water column was cooler and saltier in the CE compared to that in ACE and NE regions (Fig. 4a,b). Higher Chl-a in the upper 50 m of water column and shallower SCM were observed in the CE than in ACE region (Fig. 4c).

3.3. Spatial variations in C_T and pCO₂ in the coastal BoB

The C_T showed strong spatial variability associated with eddies (Fig. 5a). The concentration of C_T in the upper 25m of water column in the north was lower by ~120 μM than in south associated with low salinity in the north (Fig. 5a). The depth of 2100 μM of C_T contour (50-160 m) occurred within the seasonal thermocline, hence its variation represents mixing caused by eddies. Upslopping of C_T isoline of 2100 μM observed at ~50 m in the CE region was found at 100 m in the ACE_n and ACE_s regions (Fig. 5a). pH of the upper 25 m of water column was higher in the north associated with low salinity compared to that south (Fig. 5b). Upslopping of 7.8 pH isoline to 50 m was observed in the CE but the same was located at ~125 m in the rest of the study area (Fig. 5b). pCO₂ in the upper 25 m of water column in the northern BoB was lower than atmospheric value (405 μatm) and it increased to ~480 μatm in the south (Fig. 5c). Upslopping of 800 μatm of pCO₂ isolines from 175 m to 50 m was observed in the CE region (Fig. 5c).

Higher C_T, and pCO₂ and lower pH values were observed in the CE and NE regions in the upper 200 m of water column compared to that in ACE_n and ACE_s (Fig. 5a-c). Lower C_T, and higher pH waters penetrated to 150-175 m under both ACEs and the depth of penetration seems to be deeper in the ACE_n than in ACE_s. The doming of the isolines was observed up to 40 m depth (Fig. 5a). pCO₂ in the upper 40 m in the CE region was undersaturated with respect to the atmospheric pCO₂ (405±3 μatm; our unpublished data) whereas supersaturation was observed in ACE_n, ACE_s and NE regions (Fig. 5c). The C_T showed a significant inverse relation with temperature ($r^2=0.52$; $p<0.001$), salinity ($r^2=0.65$; $p<0.001$), Chl-a ($r^2=0.32$; $p<0.01$) and DO saturation ($r^2=0.38$; $p<0.01$; Fig. 6a-d) in the mixed layer. Similarly mixed layer pCO₂ displayed linear relation with salinity ($r^2=0.29$; $p<0.01$) and inverse relation with Chl-a ($r^2=0.33$; $p<0.01$) (Figure is not shown).

The monthly mean wind speeds varied between 2.85 and 8.18 m s⁻¹ in the study region (Fig. 7a). The surface pCO₂ ranged from 294 to 555 µatm and relatively lower than atmospheric value (405±3 µatm) was observed in the CE and partly ACE_s region and above atmospheric values were noticed in other regions (Fig. 7b). The sea-to-air fluxes of CO₂ were estimated using computed pCO₂ and monthly mean winds. The sea-to-air fluxes of CO₂ (Fig. 7c) ranged between -0.21 and 0.31 molC m⁻² month⁻¹ and the mean CO₂ flux from the entire study region amounted to 0.05 molC m⁻² month⁻¹ to the atmosphere.

4. Discussion

The satellite altimetry data suggests that the entire BoB is covered by several ACEs of variable sizes (400 to 600 km) and few CEs (50 to 150 km) during the study period (Fig. 1a). Dandapath and Chakraborty (2016) reported that number of CEs is less than ACEs during all seasons except in summer when the former dominates the latter. The ACE, in general, move westward, but the CEs move southwestward in the BoB (Chen et al., 2012). The ACEs are larger but the CEs have longer lifetime and are more energetic (Dandapath and Chakraborty, 2016). In order to examine the place of origin and track of advection of the present eddies, daily altimetry data have been analysed by Sarma et al. (2018). It was found that the presently sampled CE formed in the same region about 2 months before this study whereas the ACE_n seems to have formed in the northern BoB about 9 months prior to our sampling. On the other hand, the ACE_s formed near to the Andaman Sea about 4 month prior to our sampling and advected towards west (Sarma et al., 2018). Since the origin of the sampled eddies are different, the water column characteristics are expected to vary (Sarma et al., 2018). The temperature and salinity in the upper 50 m of water column increased from north to south of the transect (Fig 2a,b). Variations in the depth of D20 suggests the occurrence of divergence in CE and convergence in ACEs in the study region. Several investigators studied eddies in the BoB and suggested that these eddies are part of the large scale poleward flow of Western boundary currents (Shetye et al., 1993). Based on the wind stress curl, it was observed that divergence occurs in the CE and convergence in the ACE regions (Shetye et al., 1993; Babu et al., 2003; Gangopadhyay et al., 2013). Low saline water was observed in the upper 50 m of water column in the CE and ACE_n regions due to advection of freshwater from Ganges (Varkey et al., 1996). The depth of mixed layer was shallow (10±2 m) in the CE and NE (14±1 m) regions than in ACEs (23-28 m) (Fig. 3). The size of the ACE_n is larger (~500 km) than ACE_s (~350 km). Though SSHA shows occurrence of CE and ACE in the study region, it did not reflect in neither SST nor SSS (Fig. 1b,c). Gopalan et al. (2000) found that eddies do not extend to the surface due to strong salinity stratification which is why SSHA is suggested as a better proxy to identify eddies in the BoB than SST or SSS. Relatively

enhanced surface Chl-a was observed in the CE and NE regions suggesting supply of nutrients from subsurface layers through divergence that increased phytoplankton biomass (Fig. 2d). The enhanced Chl-a may not have advected from the western coastal BoB as the eddies were advecting from eastern BoB (Sarma et al., 2018). Both *in situ* observations and satellite imageries, indicate increase in Chl-a only in CE and NE regions, but not in ACE regions, is due to *in situ* production (Fig 1d, and 2c). Nevertheless, the hydrographic features suggest that possible occurrence of divergence in the CE whereas possible convergence in the ACE regions (Fig. 2a,b).

Relatively higher Chl-a, was observed in the upper 25 m of water column in the CE region than ACE_n, ACE_s and NE regions suggesting that increased primary productivity associated with input of nutrients to the upper ocean in the CE region (Fig. 2c) (Prasanna Kumar et al., 2004). Prominent subsurface Chl-a maxima (SCM) were observed in the entire study region but were found higher and at shallower depth in the CE than ACE_n, ACE_s and NE regions due to upwelling of subsurface waters in the CE region (Figs. 2c, and 3c). The enhanced depth integrated (up to 100 m) Chl-a in the CE compared to NE, ACE_n and ACE_s (Fig. 4b) indicate that CE is more productive than ACE due to injection of nutrients. Enhanced primary productivity by 2 to 3 times was reported in the CE than NE region in the BoB (Prasanna Kumar et al., 2004; Singh et al., 2015) further confirming that CEs are more productive.

4.2. Variations in C_T in the CE and ACE

Concentrations of C_T showed significant spatial variability in response to physical processes such as salinity, convergence/divergence in the CE and ACE (Fig. 5a). Relatively low C_T was observed in the upper 50 m of water column in the CE and ACE_n associated with low salinity in the northern Bay (Fig. 2 and 5). Perennial rivers, Ganges and Brahmaputra, discharges resulted in advection of low saline water from the coast to the study region. River water contains ~2-3 times lower concentrations of inorganic carbon than in seawater resulting in low C_T in the northern Bay (Sarma et al., 2012a,b). Kumar et al. (1996) observed lower C_T concentrations in the upper 50 m of water column associated with low salinity during winter and pre-southwest monsoon period in the BoB and lower C_T was also observed during southwest monsoon period (Sarma et al., 2012b). The linear relationship between salinity and C_T (Fig. 6b) suggests freshwater discharge controlled C_T variability in the upper ocean in the BoB. A rapid increase in C_T was observed below 50 m in the entire study region associated with increase in salinity (Fig. 2b and 5a). The variations in the 2100 μM isoline of C_T (Fig. 5a) followed the D20 isotherm (Fig. 2a). The deepening of low C_T isolines suggests that convergence of low C_T waters in the ACE regions whereas enhanced C_T concentrations were observed in the CE region due to divergence of waters (Fig. 5a).

The pH distribution pattern was opposite to those of C_T with relatively higher pH in the northern Bay that decreased towards south (Fig 5b). The pH in the Ganges estuary is higher (8.130 ± 0.24) compared to the peninsular river estuaries (7.020 to 7.470; Mukhopadhyay et al., 2002; Sarma et al., 2012a). Since the northern Bay is influenced by discharge from the Ganges river, higher pH is expected. pH showed a significant inverse relation with salinity ($r^2=0.48$; $p<0.001$) suggesting that higher pH was caused by Ganges discharge. The depth of 7.9 pH isoline followed the thermocline suggesting the influence of mixing on the distribution of pH (Fig. 5b). The pCO_2 varied between 294 and 555 μatm in the surface waters with lower levels in the northern Bay associated with low salinity (Fig. 5c). Relatively lower pCO_2 was observed in the upper 75 m depth in both ACE_n and ACE_s and enhanced pCO_2 levels were observed (up to 558 μatm) below 25 m in the CE and NE regions (Fig. 5c). The pCO_2 levels also displayed a linear relationship with salinity suggesting that pCO_2 is undersaturated with reference to atmospheric CO_2 (405 μatm) in the northern Bay due to advection of low saline water from the Ganges while supersaturated in the ACE_s and NE regions. The pCO_2 levels in the Ganges river were about 502 ± 100 μatm , which is an order of magnitude less than that of peninsular river estuaries (4981-17205 μatm ; Sarma et al., 2012a). Perennial occurrence of low pCO_2 levels, below atmospheric value, was reported in the northern Bay (Kumar et al., 1996; Sarma et al., 2012b) due to freshwater input from the Ganges river.

In order to differentiate the dominance of physical versus biological processes, C_T was normalized to constant salinity following Friis et al. (2003) and found inverse correlation with Chl-a ($r^2=0.35$; $p<0.01$; Fig. 6c) and dissolved oxygen saturation ($r^2=0.30$; $p<0.01$; Fig. 6d), which neglect the extent of biological productivity. These relationships suggest that both biological and physical processes are important in controlling C_T concentrations in the BoB. Significant correlation of C_T with Chl-a cannot be expected as C_T is also modified by heterotrophic activity and also Chl-a is not a measure of primary production as several other factors such as light, mixing, and grazing also determines primary production. On the other hand a strong negative relationship of salinity normalised C_T with DO saturation (Fig. 6d) also suggests that dominant heterotrophy controls variations in C_T in the study region. The pCO_2 also displayed negative weak relation with Chl-a ($r^2=0.33$; $p<0.01$) suggesting significant carbon removal through biological processes.

4.3. Controls of pCO_2 in the coastal BoB

In order to quantify the role of physical and biological processes on variations in pCO_2 in the BoB, the contribution of different effects on pCO_2 was estimated following the model of Louanchi et al. (1996). The changes in pCO_2 caused by biological processes such as primary production and

respiration and changes due to dissolution and precipitation of calcium carbonate (biological effect), mixing with high pCO₂ subsurface waters (mixing effect), changes in pCO₂ due to variations in solubility caused by temperature and salinity changes (thermal effect) and variations in pCO₂ due to changes in CO₂ fluxes at sea-to-air interface (flux effect) were evaluated using following equations (Louanchi et al., 1996) and presented in Fig. 8.

$$\delta C_T/\delta t = (\delta C_T/\delta t)_B + (\delta C_T/\delta t)_M + (\delta C_T/\delta t)_T + \delta C_T/\delta t)_F$$

$$\delta TA/\delta t = (\delta TA/\delta t)_B + (\delta TA/\delta t)_M$$

where subscripts B, M, T and F represents biological, mixing, thermal and flux respectively.

($\delta C_T/\delta t$)_B represents biological effect and it is computed as

$$(\delta C_T/\delta t)_B = (\delta IN/\delta t)_B * RCN - Sb$$

$$(\delta TA/\delta t)_B = -2 * Sb$$

$$(\delta IN/\delta t)_B = -(u - r * q) * Chl * N:Chl$$

where growth rate (u) was computed based on Michaelis Menten formulation (Louanchi et al., 1996). Removing factor (r) was considered as 0.5. The term Sb represents the variations in time of the global calcite concentration which is expressed as 20% of the total exported production (Broecker and Peng, 1982).

The mixing effect is computed as

$$(\delta C_T/\delta t)_M = (C_{Tb} - C_{Ts}) * \delta Z/Z_m$$

where C_{Tb} and C_{Ts} represents concentration of C_T in the below mixed layer and surface, δZ and Z_m denotes magnitudes of change in depth of mixed layer and depth of mixed layer respectively.

The thermodynamic effect is computed following Goyet et al. (1993) using change in temperature and salinity within and outside the eddy. And effect of flux was computed using following equation:

$$(\delta C_T/\delta t)_F = F/Z_m$$

where F is flux at air-sea CO₂ flux and Z_m is depth of mixed layer.

The biological effect is computed based on variations in Chl-a, dissolved inorganic nitrate within each eddy from that of outside. In this model, it is assumed that about 90% of the primary production is respired within the mixed layer and the remaining is exported to sink to the deeper depths. This assumption is reasonable based the recent sediment trap studies by Anand et al. (2017) who found

that about 85-95% of primary production is utilized within the upper ocean and ~10% of production reached the twilight zone.

This analysis suggested that biological effect and mixing effect were the dominant controlling factors followed by thermal and flux effects. Biological effect (mixing effect) decreased (increased) $p\text{CO}_2$ by 5 to 49 (5-18) μatm in the CE region whereas biological effect was significantly low in the ACE region by almost half (Fig. 7). The effect of mixing and thermal effect are significant in the ACE region where minimal biological effect was observed ($<5 \mu\text{atm}$) and it is consistent with the Chl-a distribution (Fig. 2c). On the other hand, the contribution of flux effect to variations in $p\text{CO}_2$ was relatively low due to weak winds, but it changed $p\text{CO}_2$ by 0.4 to 2.6 μatm in the study region. The effect of mixing dominated over biological effect in the CE region and these two effects were at near balance in the ACEs (Fig. 7).

4.4. Fluxes of CO_2 to the atmosphere

The wind speeds varied between 2.85 and 8.18 m s^{-1} and stronger winds were observed near the ACE regions than in the CE region (Fig. 7a). The flux of the CO_2 depends on the $p\text{CO}_2$ difference between surface waters and atmosphere and wind speed. The $p\text{CO}_2$ in the surface waters ranged between 294 and 555 μatm and lower than atmospheric values were observed in the CE and partly ACE_s region whereas above atmospheric values were observed in ACE_n and NE regions (Fig. 7b). The sea-to-air fluxes of CO_2 (Fig. 7c) varied between -0.21 and 0.31 $\text{molC m}^{-2} \text{month}^{-1}$. The CE was acting as a sink for the atmospheric CO_2 ($-0.03 \text{ molC m}^{-2} \text{month}^{-1}$) whereas ACE_n ($0.15 \text{ molC m}^{-2} \text{month}^{-1}$), ACE_s ($0.03 \text{ molC m}^{-2} \text{month}^{-1}$) and NE ($0.07 \text{ molC m}^{-2} \text{month}^{-1}$) regions were a source to the atmospheric CO_2 (Fig. 7c) The mean CO_2 flux from the entire study region suggests mild source ($0.05 \text{ molC m}^{-2} \text{month}^{-1}$) to the atmosphere.

4.5. Vertical flux of C_T

The surface water mass sinks in the ACE region due to anticyclonic circulation. This results in injection of surface C_T to the subsurface waters. In order to quantify this, vertical flux of C_T was computed. It has been proposed that vertical turbulent diffusion (K_z) depends inversely on the vertical stability ($N^2 = g(\partial\rho/\partial z)/\rho$) at away from the sources and sinks of turbulence, and for negligible shear (Welander, 1968; Sarmiento et al., 1976). Since silica dissolution occurs at greater depth (Broecker and Peng, 1982), due to high pressure, no marked decrease in the amount of opal was found as a function of depth in the sediment traps in the North Pacific (Broecker and Peng, 1982; Wong et al., 1999; Honda et al., 2002). Hence the analytical expression for the dependence between

K_z and the vertical stability can be obtained. In the 100-500 m the relation between $\partial\text{SiO}_4/\partial z$ and N^2 is linear, thus

$$K_z = a \cdot N^2$$

Based on the relation between N^2 and $\partial\text{SiO}_4/\partial z$, the constant 'a' was computed to be $3.4 \pm 0.4 \times 10^9 \text{ m}^2 \text{ s}^{-3}$. The mean N^2 in the 100-500 m depth is $9.1 \pm 1.0 \times 10^{-5} \text{ s}^{-2}$ and thus the average K_z was $3.7 \pm 1.2 \times 10^{-5} \text{ m}^2 \text{ s}^{-1}$. The computed K_z is about two times higher than the coefficient of the vertical diffusion estimated by Matear and Wong (1997) ($K_z \sim 1.5 \times 10^{-5} \text{ m}^2 \text{ s}^{-1}$) in the North Pacific.

The diapycnal flux of the dissolved element (say C_T) can be computed as

$$F = a \cdot (\partial C / \partial z) \cdot N^2$$

Based on this, the flux of C_T was computed in the ACE_n, ACE_s and CE regions. The mean vertical flux of C_T in the ACE_n and ACE_s was $0.07 \pm 0.02 \text{ molC m}^{-2} \text{ month}^{-1}$ whereas it was $\sim 0.02 \pm 0.006 \text{ molC m}^{-2} \text{ month}^{-1}$ in the CE and NE regions. This study suggests that significant amount of C_T is exported to the subsurface zone by ACEs. The computed vertical flux of C_T at the upper boundary of the intermediate layer of ACE was almost $\sim 85\%$ of the sea-air flux of CO_2 to the atmosphere ($0.08 \pm 0.03 \text{ mol C m}^{-2} \text{ month}^{-1}$ in the both the ACEs). However, it acted as a sink region due to freshwater lens resulted from river discharge. The behaviour of CEs in the southern BoB may be different due to less impact of freshwater. This study suggests that western BoB is a source for the atmospheric CO_2 , however, the ACE are pumping significant amount of CO_2 to the subsurface waters. Chen et al. (2012) identified 4,701 and 4,713 ACEs and CEs in 532 and 525 tracks, respectively, between 1992 and 2009. Dandapath and Chakraborty (2016) reported that number of CEs is less than the ACEs during all seasons except summer in the BoB. To account the strength of BoB as a source or sink, the influence of meso-scale features must be considered. In order to estimate the contribution of C_T flux to the subsurface waters, the same is estimated considering all eddies, formed in one year in the BoB, assuming that the C_T flux rates estimated in the sampled eddies are same for other eddies as well. The number of eddies formed in the BoB is estimated using monthly mean SSHA and area of eddy was computed based on the area covered by 0.2 m of SSHA contour for ACE and -0.2 m for CE (Supplimentary Figure S1). The total areas covered by ACE and CE in a year were estimated to be 3.9 and $0.2 \times 10^{12} \text{ m}^2$, respectively. Using the mean C_T flux of 0.07 ± 0.02 and $0.02 \pm 0.006 \text{ molC m}^{-2} \text{ month}^{-1}$ at ACE and CE regions, the annual flux of C_T to deep water estimated to be 0.27×10^{12} and $0.004 \times 10^{12} \text{ mole C y}^{-1}$, respectively in the ACE and CE regions. The total C_T flux to deep BoB by ACE and CE amounted to $3.29 \pm 0.9 \text{ TgC y}^{-1}$ ($1 \text{ Tg} = 10^{12} \text{ gC}$). However, these estimates must be considered as conservative as C_T flux depends on the eddy

origin and concentrations of C_T concentrations in the eddy and Kz. Therefore a combination of continuous monitoring for the carbonate parameters in the eddies and numerical modelling will help to quantify C_T flux to the subsurface layers by the eddies and CO_2 fluxes at the sea-to-air interface.

5. Summary and Conclusion

Variations in hydrography and total inorganic carbon (C_T) components were measured in the western Bay of Bengal (BoB) covering two anticyclonic (ACE_n and ACE_s), cyclonic (CE) and no eddy (NE) regions to examine the influence of eddies on C_T components. The depth of 20° C isotherm (D20) was located at ~80 m in the CE and the same deepened to ~180 m in the ACE_n and ACE_s . The ACE_n and CE were formed in the northern Bay about 9 months prior to our sampling whereas the ACE_s was formed 4 months prior to our sampling in the eastern BoB and advected to the study region. Both surface and depth integrated Chl-a to 100 m was higher in the CE region than in ACEs and NE regions. Upslopping of high C_T , and pCO_2 isolines from the depth of 175 m was observed in the northern Bay associated with CE resulting in the increase in C_T and pCO_2 , respectively, in the CE compared to NE region. Relatively lower C_T , and higher pH waters penetrated to 150-175 m under the ACE_n and ACE_s influence. Moderate inverse correlation with Chl-a and dissolved oxygen saturation with salinity normalized C_T suggests both biological and physical processes are important in controlling C_T in the BoB. Both biological effect and mixing effect contributed significantly to pCO_2 levels in the CE region whereas mixing and thermal effect contributed in the ACE region. The sea-to-air fluxes of CO_2 varied between -0.3 and 0.4 molC m⁻² month⁻¹ and CE and ACE_s regions were acting as a sink for the atmospheric CO_2 whereas ACE_n and NE regions are source to the atmospheric CO_2 . The mean CO_2 flux suggests that the study region is a moderate source of CO_2 (0.05 ± 0.01 mol C m⁻² month⁻¹) to the atmosphere. The mean vertical flux of C_T to the deeper layer in the ACE_n and ACE_s was 0.07 ± 0.02 mol C m⁻² month⁻¹ whereas it was $\sim 0.02 \pm 0.006$ molC m⁻² month⁻¹ in the CE and NE regions. This study suggests that eddies transport C_T to deeper waters and efflux CO_2 to the atmosphere in the BoB. The role of meso-scale eddies must be considered in order to evaluate the net flux of CO_2 from the BoB.

Acknowledgements: We would like to thank Director, CSIR-National Institute of Oceanography for this constant encouragement and support. We would like to thank three anonymous reviewers for their constructive comments and suggestion to improve the presentation of manuscript. We would like to thank funding agency - INCOIS, Ministry of Earth Science for sponsoring this work through O-MASCOT project. We would appreciate the help tendered by Ship cell, and ship staff during sampling. This has NIO contribution number.....

References

- Babu, M. T., Sarma, Y. V. B., Murty, V. S. N. and Vethamony, P., 2003. On the circulation in the BoB during Northern spring inter-monsoon (March-April 1987). *Deep Sea Res. Part II.* **50**, 855-865.
- Bauer, J. E., Cai, W.-J., Raymond, P. A., Bianchi, T. S., Hopkinson, C. S., and Regnier, P. A. G., 2013. The changing carbon cycle of the coastal ocean. *Nature*. **504**, 61–70.
- Borges, A.V., 2005. Do we have enough pieces of the jigsaw to integrate CO₂ fluxes in the coastal ocean. *Estuaries*. **28**, 3-27.
- Carpenter, J.H., 1966. New measurements of oxygen solubility in pure and natural waters. *Limnology and Oceanography*. **11**, 264-277.
- Chen, G., D. Wang, and Y. Hou (2012). The features and interannual variability mechanism of mesoscale eddies in the Bay of Bengal. *Cont. Shelf Res.*, **47**, 178-185.
- Chen, C.T. A., Huang, T.-H., Chen, Y.-C., Bai, Y., He, X., and Kang, Y., 2013. Air-sea exchanges of CO₂ in the world's coastal seas. *Biogeosciences*. **10**, 6509–6544, doi:10.5194/bg-10-6509.
- Dandapat, S., Chakraborty, A. (2016). Mesoscale eddies in the Western Bay of Bengal as observed from satellite altimetry in 1993-2014: Statistical characteristics, variability and three-dimensional properties. *IEEE J. Appl. Earth Obser. Remote Sens.*, doi: 10.1109/JSTARS.2016.2585179.
- Friis, K., Körtzinger, A. and Wallace, D.W.R., 2003. The salinity normalization of marine inorganic carbon chemistry data. *Geophys. Res. Lett.* **30** (2), 1085. doi:10.1029/2002GL015898.
- Gangopadhyay, A., Bharatraj, G.N., Chaudhuri, A.H., Babu, M.T., Sengupta, D., 2013. On the nature of meandering of the springtime western boundary current in the Bay of Bengal. *Geophys. Res. Lett.* **40**, 2188–2193. doi:10.1002/grl.50412.
- Gnanadesikan, A., Pradal, M.A., and Abernathey, R. 2015. Isopycnal mixing by mesoscale eddies significantly impacts oceanic anthropogenic carbon uptake. *Geophys. Res. Lett.*, **42**, 4249-4255.
- Gonzalez-Davila, M., Santana-Casiano, J.M., Armas, D.D., Escanez, J., and Suarez-Tangil, M. 2006. The influence of island generated eddies on the carbon dioxide system, South of the Canary Islands, *Mar. Chem*, **99**, 177-190.
- Gopalan, A.K.S., V.V. Gopalakrishna, M.M. Ali, and R. Sharma (2000). Detection of Bay of Bengal eddies from TOPEX and in situ observations. *J. Mar. Res.*, **58**, 721-734.
- Gopalakrishna, V.V. and J.S. Sastry, J.S., 1985. Surface circulation over the shelf off the east coast of India during the southwest monsoon. *Indian J. Mar. Sci.* **14**, 62-65.
- Grasshoff K, Ehrhardt M and Kremling K (eds) 1983. *Methods of Seawater Analysis*; Weinheim: *Verlag Chemie*, pp. 89–224.
- International Geosphere Biosphere Program (IGBP)., 1993. *Land-Ocean Interactions in the Coastal Zone*, Science Plan. IGBP of ICSU, Report no.25, Stockholm, 50 pp.

- Ittekkot, V., Nair, R. R., Honjo, S., Ramaswamy, V., Bartsch, M. and co-authors., 1991. Enhanced particle fluxes in Bay of Bengal induced by injection of fresh water. *Nature*.**351**, 385-387.
- Kimura, K. 1970. A mechanism of fishing ground formation due to warm eddies cut off from the Kuroshio Front. *Mar. Sci. Mon.*, 5, 35-47.
- Kumar, M.D., Naqvi, S.W.A., George, M.D., Jayakumar, D.A., 1996. A sink for atmospheric carbon dioxide in the northeast Indian Ocean. *J. Geophys. Res.***101**, 18121-18125.
- Kusakabe, M., Andreev, A., Lobanov, V., Zhabin, I., Kumamoto, Y., and Murata, A. 2002. Effects of the anticyclonic eddies on water masses, chemical parameters and chlorophyll distributions in the Oyashio current region, *J. Oceanogr.*, 58, 691-701.
- Laruelle, G. G., Durr, H. H., Slomp, C. P. and Borges, A. V., 2010. Evaluation of sinks and sources of CO₂ in the global coastal ocean using a spatially-explicit typology of estuaries and continental shelves. *Geophys. Res. Lett.* **37**, L15607.
- Laruelle, G. G., Lauerwald, R., Pfeil, B., and Regnier, P., 2014. Regionalized global budget of the CO₂ exchange at the air-water interface in continental shelf seas. *Global Biogeochem. Cy.***28**, 1199–1214, doi:10.1002/2014GB004832.
- Lewis, E., Wallace, D. W. R., 1998. Program Developed for CO₂ System Calculations. Carbon Dioxide Information Analysis Center, Oak Ridge National Laboratory, U.S. Department of Energy, Oak Ridge, TN. ORNL/CDIAC-105.
- Louanchi, F., Metzli, N., and Poisson, A., 1996. Modelling the monthly sea surface pCO₂ fields in the Indian Ocean. *Mar. Chem.* **55**, 265–279.
- Millero, F. J., Graham, T. B., Huang, F., Bustos-Serrano, H., Perrot, D., 2006. Dissociation constants of carbonic acid in seawater as a function of salinity and temperature. *Mar. Chem.* **100**, 80-94.
- Mukhopadhyay, S. K., Biswas, H., De, T. K., Sen, S. and Jana, T. K., 2002. Seasonal effects on the air-water carbon dioxide exchange in the Hooghly estuary, NE coast of Bay of Bengal, India. *J. Environ. Monit.***4**, 549-552.
- Murty, V. S. N., Suryanarayana, A. and Rao. D. P., 1993. Current structure and volume transport across 12°N in the Bay of Bengal. *Indian J. Mar. Sci.* **22**, 12–16.
- Narvekar, J. and S.P. Prasanna Kumar.(2007). Seasonal variability of the mixed layer in the central Bay of Bengal and associated changes in nutrients and chlorophyll. *Deep-Sea Res., I*, 53, 820-835.
- Perez, F.F., Mintrop, L., Llinas, O., Gonzalez-Davila, M., Castro, C.G., Alvarez, M., Kortzinger, A., Santana-Casiano, M., Rueda, M.J., Rios, A.F. 2001. Mixing analysis of nutrients, oxygen and inorganic carbon in the Canary Islands region. *J. Mar. Syst.*, 28, 183-201.
- Prasanna Kumar, S.P., M. Nuncio, J. Narvekar, A. Kumar, S. Sardesai, S.N. De Sousa, M. Gauns, N. Ramaiah, and M. Madhupratap. (2004). Are eddies nature's trigger to enhance biological productivity in the Bay of Bengal? *Geophys. Res. Lett.*, 31, L07309, doi: 10.1029/ 2003GL019274.

- Regnier, P., Friedlingstein, P., Ciais, P., Mackenzie, F. T., Gruber, N., Janssens, I., Laruelle, G. G., Lauerwald, R., Luysaert, S., Andersson, A. J., Arndt, S., Arnosti, C., Borges, A. V., Dale, A. W., Gallego-Sala, A., Godd ris, Y., Goossens, N., Hartmann, J., Heinze, C., Ilyina, T., Joos, F., LaRowe, D. E., Leifeld, J., Meysman, F. J. R., Munhoven, G., Raymond, P. A., Spahni, R., Suntharalingam, P. and Thullner, M., 2013. Anthropogenic perturbation of the carbon fluxes from land to ocean. *Nat. Geosci.* **6**, 597–607, doi:10.1038/ngeo1830.
- Rogachev, K.A., Tishchenko, P.Y., Pavlova, G.Y., Bychkov, A.S., Carmack, E.C., Wong, C.S., and Yurasov, G.I. 1996. The influence of fresh-core rings on chemical concentrations (CO₂, PO₄, O₂, alkalinity, and pH) in the western subarctic Pacific Ocean. *J. Geophys. Res.*, 101, 999-1010.
- Sanilkumar, K.V., Kuruvilla, T.V., Jogendranath, D. and Rao, R.R., 1997. Observations of the Western Boundary Current of the Bay of Bengal from a hydrographic survey during March 1993. *Deep-Sea Res. I*, **44** (1), 135-145.
- Sarma, V. V. S. S., 1998. Variability in Forms and Fluxes of Carbon Dioxide in the Arabian Sea. PhD Thesis. Goa University, Goa, India, pp. 1-256 (*unpublished*)
- Sarma, V. V. S. S., Kumar, M. D., Gauns, M., and Madhupratap, M., 2000. Seasonal controls on surface pCO₂ in the central and eastern Arabian Sea. *Proc. Indian Acad. Sci. (Earth Planet. Sci.)*, **109**, 471–479.
- Sarma, V. V. S. S., Gupta, S. N. M., Babu, P. V. R., Acharya, T., Harikrishnachari, N. and co-authors., 2009. Influence of river discharge on plankton metabolic rates in the tropical monsoon driven Godavari estuary, India. *Estuar. Coastal Shelf Sci.* **85**, 515-524.
- Sarma, V. V. S. S., Krishna, M. S., Rao, V. D., Viswanadham, R., Kumar, N. A., Kumai, V. R et al., 2012. Sources and Sinks of CO₂ in the west coast of Bay of Bengal. *Tellus B.***64**, 10961, doi: 3402/tellusb.v64i0.10961.
- Sarma, V. V. S. S., Viswanadham, R., Rao, G. D., Kumar, B. S. K., Prasad, V. R., Naidu, S. A., et al., 2012b. Carbon dioxide emissions from Indian monsoonal Estuaries. *Geophys. Res. Lett.* **39**, doi:10.1029/2011GL050709.
- Sarma, V.V.S.S., Krishna, M.S., Viswanadham, R., Rao, G.D., Rao, V.D., Sridevi, B., Kumar, B.S.K., Prasad, V.R., Subbaiah, Ch.V., Acharyya, T. and Bandopadhyay, D., 2013b. Intensified oxygen minimum zone on the western shelf of BOB during summer monsoon: influence of river discharge. *J. Oceanogr.***69**(1), 45–55.
- Sarma, V.V.S.S., Sridevi, B., Maneesha, K., Sridevi, T., Naidu, S.A., Prasad, V.R., Venkataramana, V., Acharya, T., Bharati, M.D., Subbaiah, C.V., Kiran, B.S., Reddy, N.P.C., Sarma, V.V., Sadharam, Y., Murty, T.V.R., 2013a. Impact of atmospheric and physical forcings on biogeochemical cycling of dissolved oxygen and nutrients in the coastal Bay of Bengal. *J. Oceanogr.* **69**(2), 229-243.
- Sarma, V. V. S. S., Krishna, M. S., Paul, Y. S. and Murthy, V. S. N., 2015. Observed changes in ocean acidity and carbon dioxide exchange in the coastal Bay of Bengal - a link to air pollution. *Tellus B.* **67**, 24638.
- Sarma, V.V.S.S., Paul, S., Vani, G.D., and Murty, V.S.N. 2015. Impact of river discharge on the coastal water pH and pCO₂ levels during the Indian Ocean Dipole (IOD) years in the western Bay of Bengal, *Continental Shelf Research*, 107, 132-140.

- Sarma, V.V.S.S., G.D. Rao, R. Viswanadham, C.K. Sherin, J. Salisbury, M.M. Omand, A. Mahadevan, V.S.N. Murty, E.L. Shroyer, M. Baumgartner, K.Stafford., 2016. Effects of freshwater stratification on nutrients, dissolved oxygen and phytoplankton in the Bay of Bengal.*Oceanogra.*, 29, 126-135.
- Shetye, S. R., Shenoi, S.S.C., Gouveia, A. D., Michael, G.S., Sundar, D. and Nampoothiri, G. 1991. Wind driven coastal upwelling along the western boundary of the Bay of Bengal during the southwest monsoon.*Cont. Shelf Res.* **11**, 1397-1408.
- Shetye, S. R., Gouveia, A.D., Shenoi, S.S.C., Sundar, D. Michael, G.S. and Nampoothid, G.,1993. The western boundary current of the seasonal subtropical gyre in the Bay of Bengal. *J.Geophys. Res.***98**, 945-954.
- Shetye, S. R., Gouveia, A. D., Shankar, D., Shenoi, S. S. C., Vinayachandran, P. N. and co-authors., 1996. Hydrography and circulation in the western Bay of Bengal during the northeast monsoon.*J.Geophys. Res.* **101**, 14011-14025.
- Suzuki, R. and Ishimaru, T.,1990. An improved method for the determination of phytoplankton chlorophyll using N,N-dimethylformamide. *J. Oceanogr.* **46**, 190-194.
- Tsunogai, S., Watanabe, S. and Sato, T., 1999. Is there a “continental shelf pump” for the absorption of atmospheric CO₂?*Tellus B.* **51**, 701-712.
- UNESCO, 1979. Discharge of Selected Rivers of the World. UNESCO, Paris.
- Varkey, M. J., Murthy, V. S. N. and Suryanarayana, A., 1996. Physical Oceanography of the Bay of Bengal and Andaman Sea.*Oceanogr. Marine Biol.: an Annual Rev.* (eds). A.D. Ansell, R.N. Gibson and Margaret Barnes, **34**, 1-70.
- Vidya, P.J., and S. Prasanna Kumar. (2013). Role of mesoscale eddies on the variability of biogenic flux in the northern and central Bay of Bengal. *J. Geophys. Res.*, *118*, 5,760–5,771, <http://dx.doi.org/10.1002/jgrc.20423>.
- Wanninkhof, R., 2014. Relationship between wind speed and gas exchange over the ocean revisited. *Limnol.Oceanogr.Methods*, doi:10.4319/lom.2014.12.351.

Legend to figures

Figure 1: The map showing weakly mean (24 to 30th March 2018) a) Sea surface height anomaly (m; color code) overlaid by geostrophic currents, b) Sea surface temperature, c) Sea surface salinity and d) monthly mean (1-31st March 2018) sea surface chlorophyll-a in the Bay of Bengal. The station locations and their numbers are also shown. The sampled eddies were also marked for identification. The data were obtained from <http://marine.copernicus.eu/services-portfolio/access-to-products/>.

Figure 2: Spatial variations in a) Temperature ($^{\circ}\text{C}$), b) salinity, c) Chlorophyll-a (mg m^{-3}) and d) dissolved oxygen (μM) along the transect in the Bay of Bengal. The station numbers are given on the upper x-axis and distance (km) from station 1 to 22 are given in the bottom x-axis. The regions of CE, ACE_n, NE and ACE_s were identified on the upper axis.

Figure 3: Spatial variations in depth of mixed layer and depth integrated (0 to 100m) Chlorophyll-a along the transect.

Figure 4: Mean vertical variations in a) temperature ($^{\circ}\text{C}$), b) salinity, c) chlorophyll-a (mg m^{-3}), d) DIC (μM), e) pH and f) pCO₂ (μatm) in the ACE (Stn. 9-11 and 18-21; red), CE (Stn. 2-4; green) and NE (Stn. 14-15; black) regions.

Figure 5: Spatial variations in a) C_T (μM), b) pH and c) pCO₂ (μatm) along the cruise track in the Bay of Bengal. The station numbers are given on the upper x-axis and distance (km) from station 1 to 22 are given in the bottom x-axis. The regions of CE, ACE_n, NE and ACE_s were identified on the upper axis.

Figure 6: Relationship of C_T with a) Temperature, b) Salinity, c) Chlorophyll-a and d) DO saturation in the mixed layer.

Figure 7: Spatial variations in a) monthly mean wind speed, b) surface pCO₂ and c) CO₂ fluxes at the sea-to-air interface along the cruise track.

Figure 8: Spatial variations in the controlling factors – biological effect (green), mixing effect (blue), thermal effect (red) and flux effect (black) – of pCO₂ along the Bay of Bengal.

Figure 1:

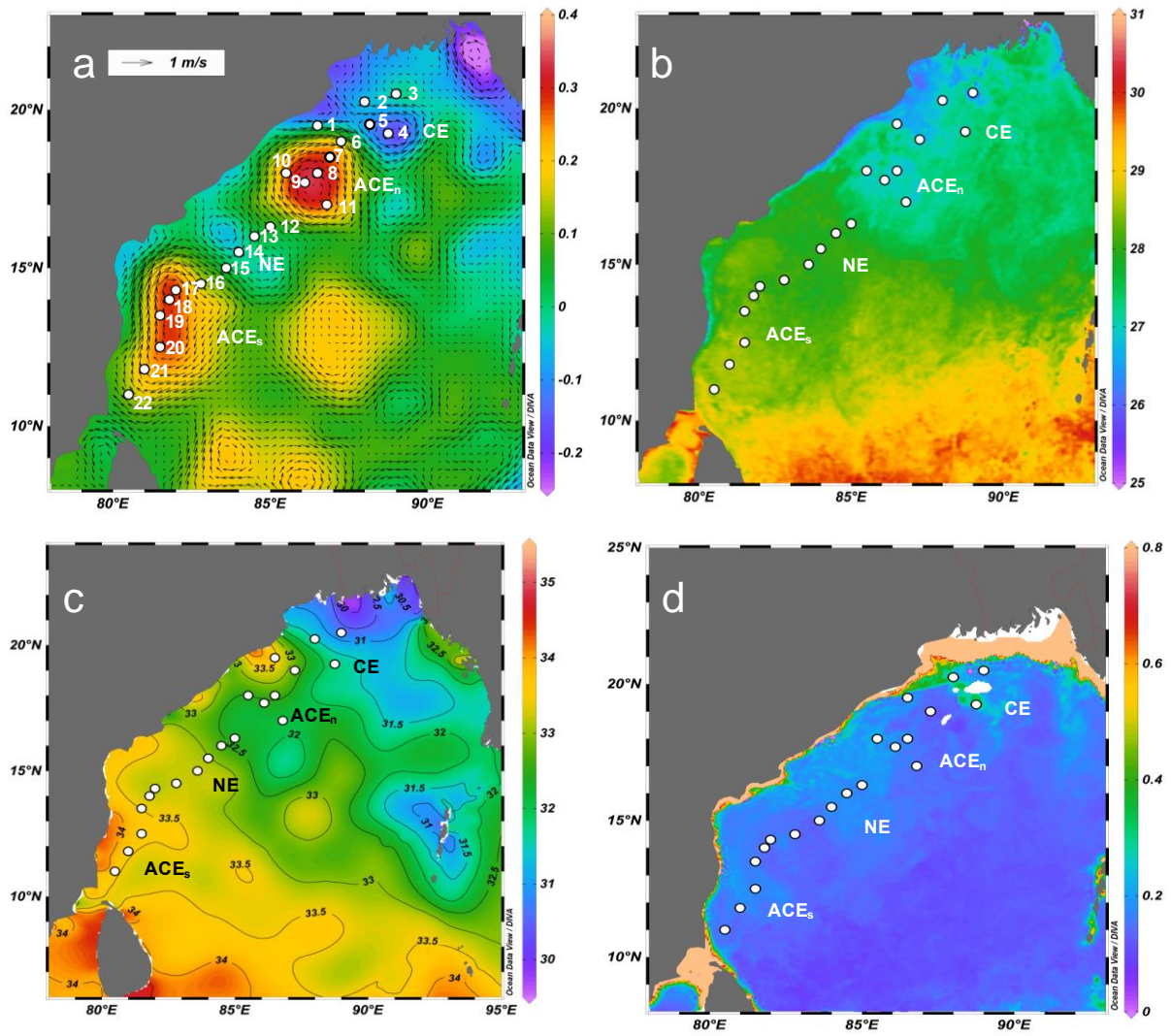


Figure 2

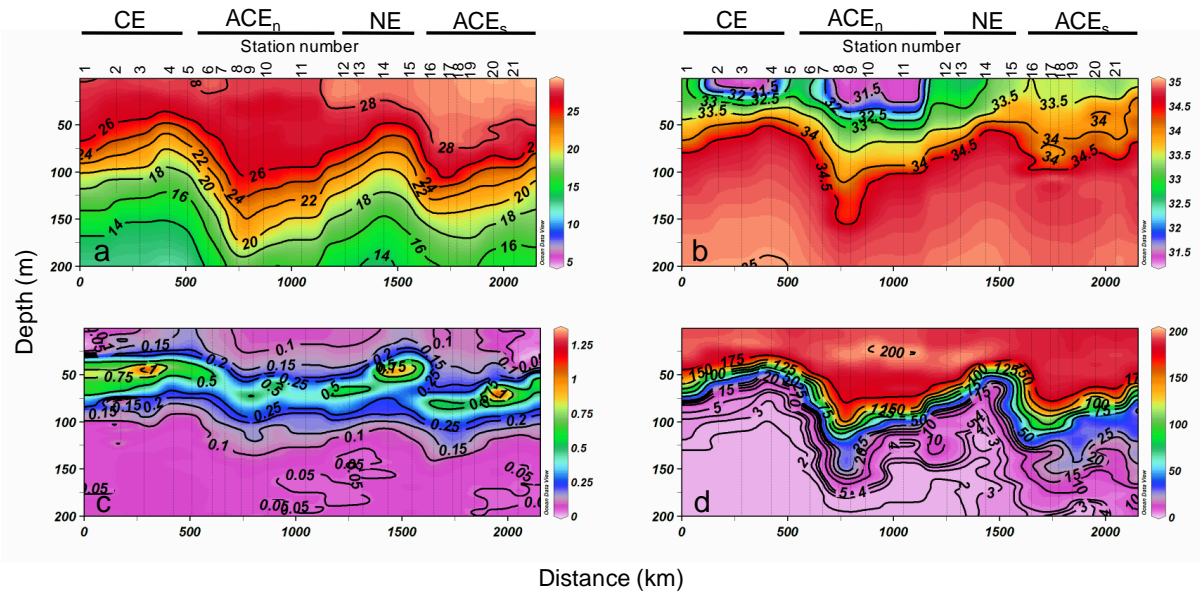


Figure: 3

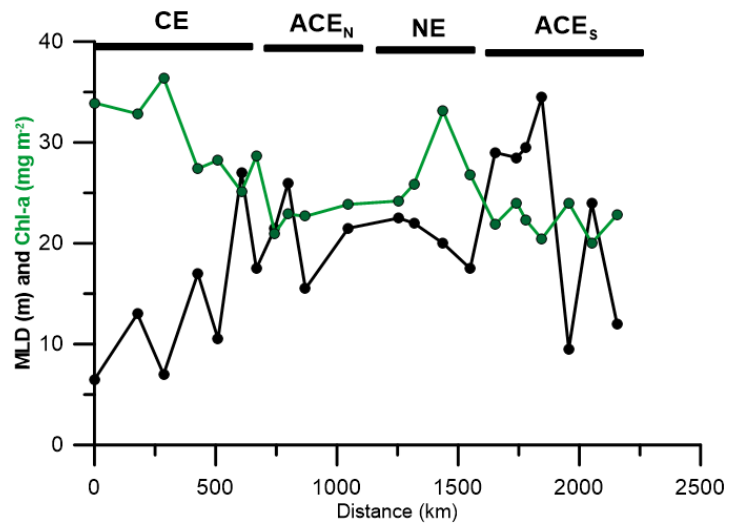


Figure 4:

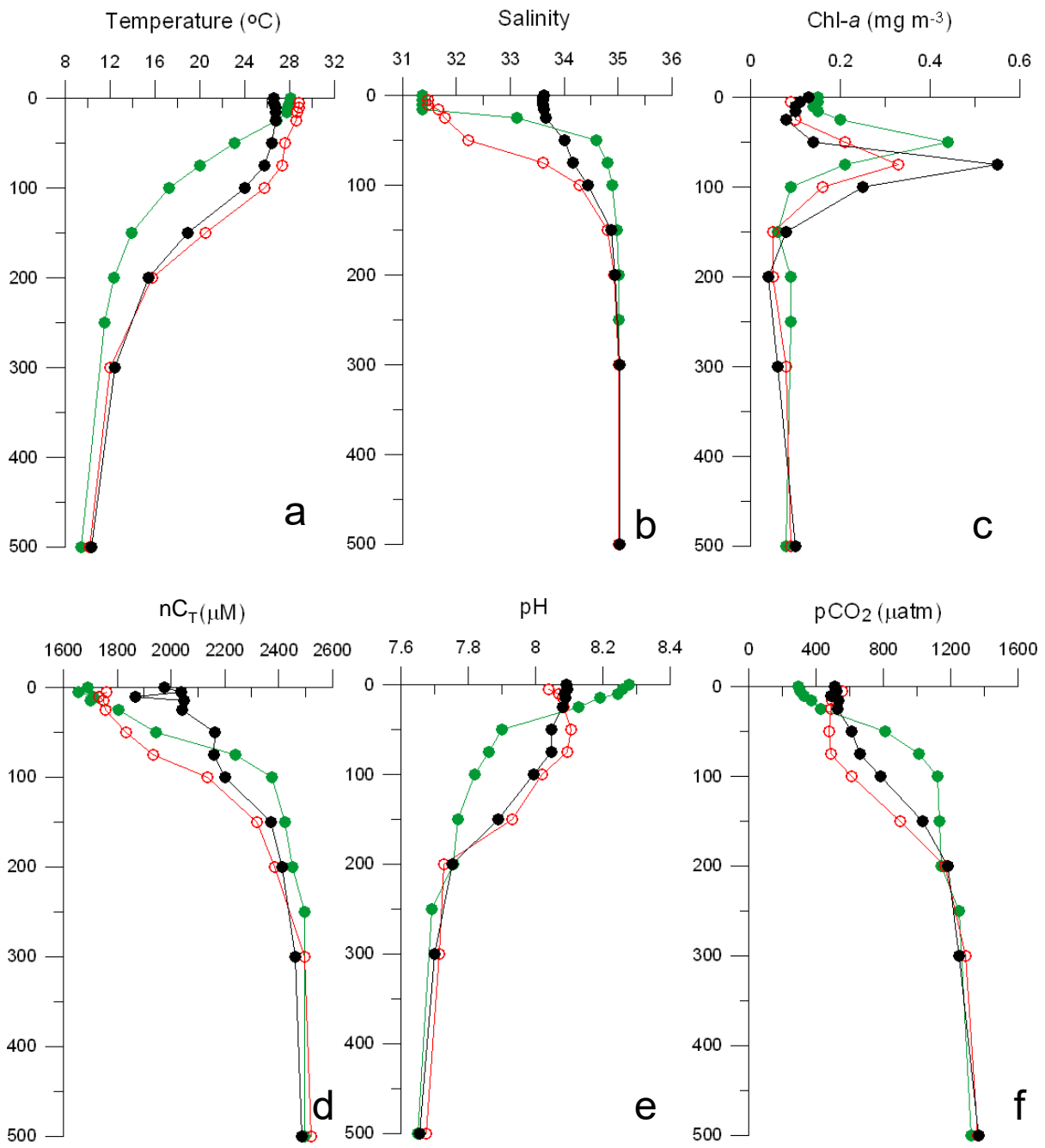


Figure 5:

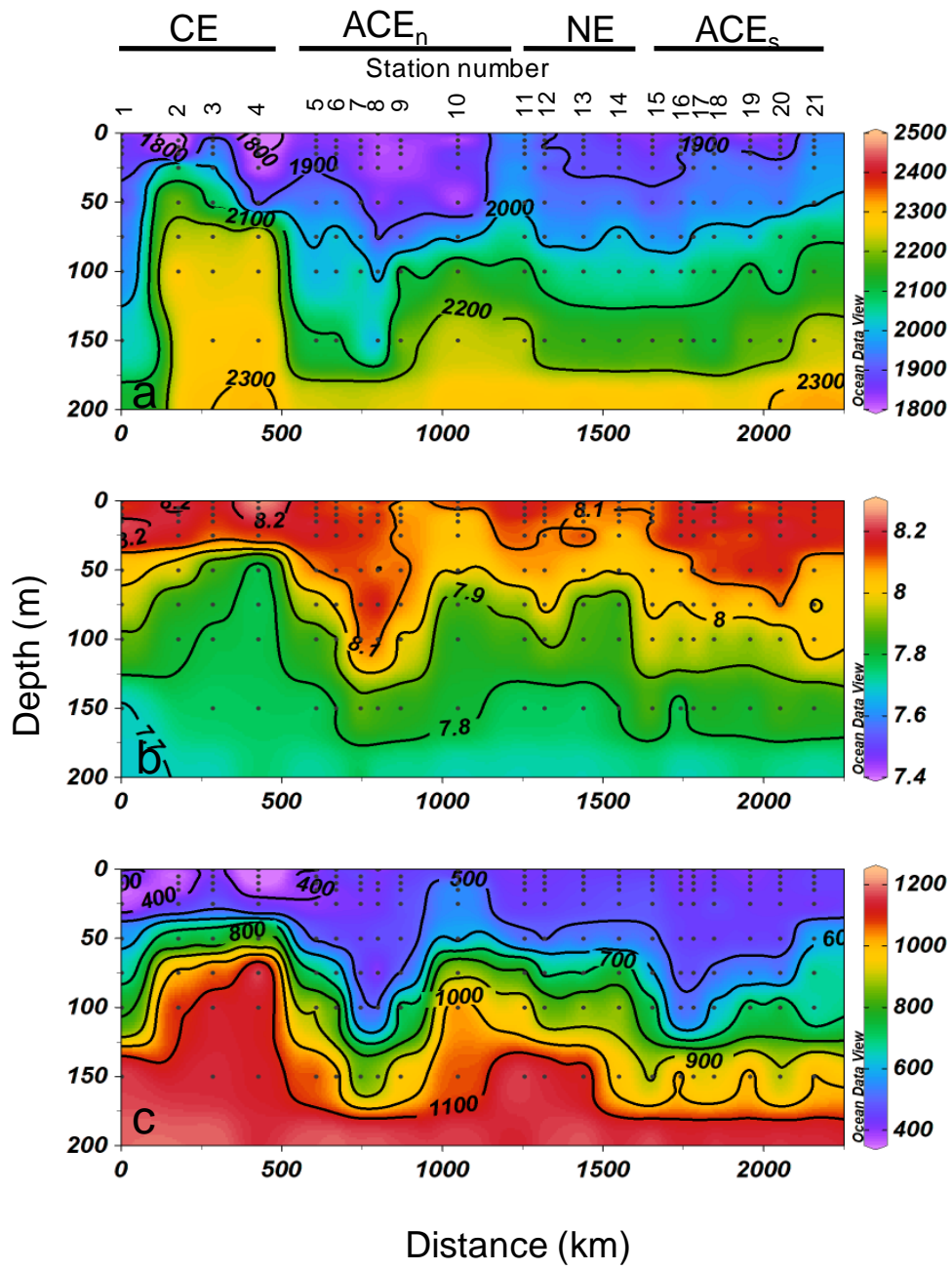


Figure 6:

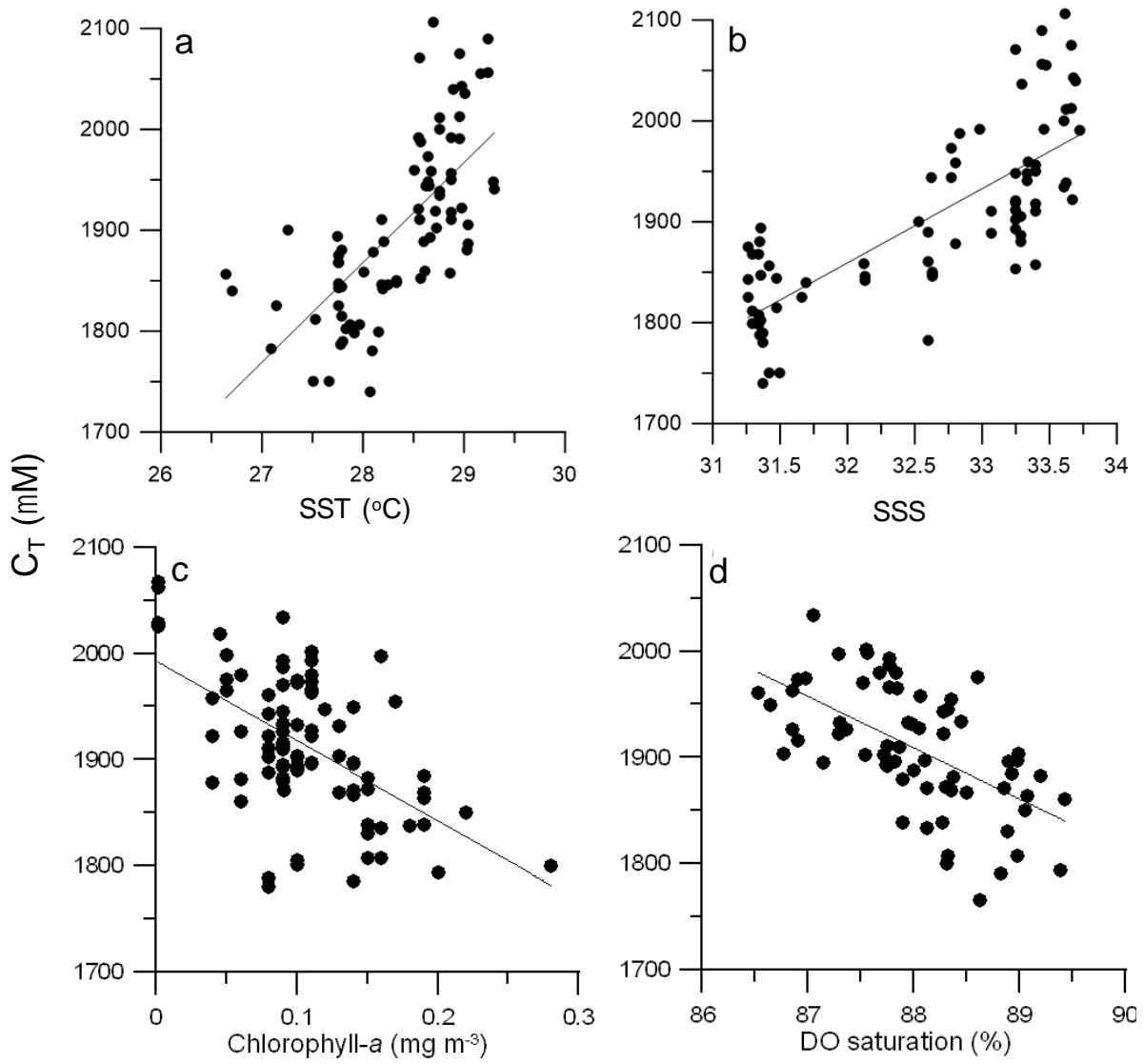


Figure 7:

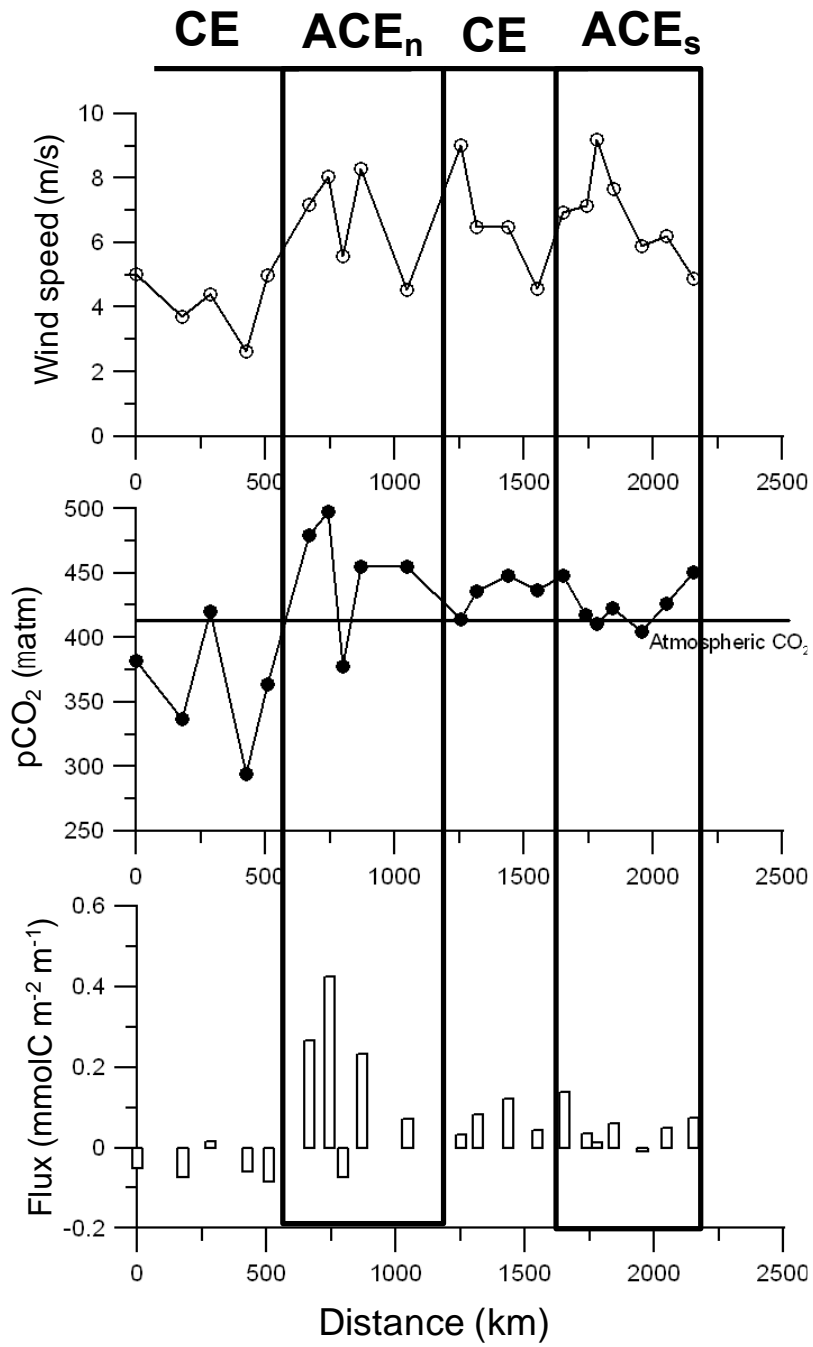


Figure 8:

